nature communications

Article

https://doi.org/10.1038/s41467-025-57793-8

HSD17B4 deficiency causes dysregulation of primary cilia and is alleviated by acetyl-CoA

Received: 20 November 2023

Accepted: 2 March 2025

Published online: 18 March 2025

Check for updates

Ji-Eun Bae[1,7], Soyoung Jang[1,2,7], Joon Bum Kim[2], Na Yeon Park[1,2], Doo Sin Jo[3], Hyejin Hyung[2], Pansoo Kim[3], Min-Seon Kim[4], Hong-Yeoul Ryu[2,5], Hyun-Shik Lee[2,5], Dong-Seok Lee[2], Myriam Baes[6], Zae Young Ryoo[2] ✉ & Dong-Hyung Cho[1,2,3] ✉

Primary cilia are dynamic sensory organelles orchestrating key signaling pathways, and disruption of primary ciliogenesis is implicated in a spectrum of genetic disorders. The peroxisomal bifunctional enzyme HSD17B4 is pivotal for peroxisomal β-oxidation and acetyl-CoA synthesis, and its deficiency profoundly impairs peroxisomal metabolism. While patients with *HSD17B4* deficiency exhibit ciliopathy-like symptoms due to dysfunctional primary cilia, the molecular connection between *HSD17B4* and ciliopathy remains poorly understood. Here, we demonstrate that *HSD17B4* deficiency impairs primary ciliogenesis and alters cilia-mediated signaling, suggesting a potential link between peroxisomal metabolism and ciliary function. Notably, elevation of acetyl-CoA rescues ciliary defects via HDAC6-mediated ciliogenesis in *HSD17B4*-deficient cells. Strikingly, acetate administration restores motor function, enhances primary cilia formation, and preserves the Purkinje layer in *Hsd17B4*-knockout mice. These findings provide insights into the functional link between *HSD17B4* and primary cilia, highlighting acetyl-CoA as a potential therapeutic target for *HSD17B4* deficiency and ciliopathy.

The primary cilia, present on the cell surface of various tissues, are highly dynamic sensory organelles that play crucial roles in mediating multiple extra- and intracellular signaling pathways, including Sonic hedgehog (Shh), transforming growth factor β (TGF-β), and platelet-derived growth factor receptor α (PDGFRα) signaling, to regulate various cellular processes[1,2]. Primary ciliogenesis, the process of primary cilia formation, is influenced by extracellular factors, such as cell culture condition through serum withdrawal[3]. Conversely, ciliary disassembly can be induced by signaling pathways, including histone deacetylase 6 (HDAC6)-mediated tubulin deacetylation, which leads to destabilization of the ciliary axoneme[4]. Disruptions in ciliogenesis and ciliary function are implicated in a range of human diseases, collectively termed ciliopathies, which include retinal degeneration, polycystic kidney disease, and various genetic disorders[5,6]. Given the diverse roles of primary cilia across multiple tissues and organ systems, ciliopathies often present with heterogeneous clinical manifestations.

Beyond its pivotal role in genetic disorders, ciliary dysfunction has been increasingly recognized as a key factor in neuronal survival and brain development[7]. Consequently, the regulation of primary ciliogenesis has emerged as a potential therapeutic strategy for ciliopathies. Interestingly, recent studies have indicated that peroxisomes are involved in trafficking cholesterol to the cilium, establishing a functional link between peroxisomal metabolism and primary cilia[8,9]. Thus, peroxisomal dysfunction may impair primary ciliogenesis. Peroxisomes are essential for lipid metabolism, particularly fatty acid β-oxidation, which results in the production of acyl-CoAs, including acetyl-CoA. Peroxisomal

[1]Organelle Institute, Kyungpook National University, Daegu, Republic of Korea. [2]School of Life Sciences, BK21 FOUR KNU Creative BioResearch Group, Kyungpook National University, Daegu, Republic of Korea. [3]ORGASIS Corp, Suwon, Gyeonggi-do, Republic of Korea. [4]Division of Endocrinology and Metabolism, Asan Medical Center, Seoul, Republic of Korea. [5]KNU G-LAMP Project Group, KNU Institute of Basic Sciences, Kyungpook National University, Daegu, Republic of Korea. [6]Laboratory of Cell Metabolism, Department of Pharmaceutical and Pharmacological Sciences, KU Leuven, Leuven, Belgium. [7]These authors contributed equally: Ji-Eun Bae, Soyoung Jang. ✉e-mail: jaewoong64@knu.ac.kr; dhcho@knu.ac.kr

β-oxidation plays a critical role in degradation of very-long-chain fatty acids (VLCFAs), which is catalyzed by multiple enzymes in distinct pathways, and contributes to the synthesis of polyunsaturated fatty acids and bile acids[10,11]. The peroxisomal β-oxidation pathway proceeds in four sequential reactions, i.e., dehydrogenation, hydration, dehydrogenation, and thiolytic cleavage, each of which is catalyzed by distinct enzymes, including acyl-CoA oxidase (ACOX1) and hydroxysteroid 17-beta dehydrogenase 4 (HSD17B4)[10,12]. Acetyl-CoA, a key product of peroxisomal β-oxidation, functions as an energy source, a lipid biosynthesis precursor, and a substrate of histone acetyltransferases (HATs) for the regulation of gene expression[13]. Therefore, abnormal β-oxidation can lead to acetyl-CoA depletion, resulting in an impaired energy supply. HSD17B4, also known as peroxisomal multifunctional protein 2 or D-bifunctional protein, is a key enzyme in peroxisomal β-oxidation, catalyzing the second and third reactions required for breakdown of VLCFAs and the production of acyl-CoA and acetyl-CoA[10,12]. Therefore, *HSD17B4* deficiency disrupts peroxisomal β-oxidation, leading to acetyl-CoA deprivation and metabolic dysfunction. The *HSD17B4* deficiency (MIM 261515) is a rare genetic disorder caused by biallelic pathogenic variants, often leading to early mortality due to severe peroxisomal metabolic dysfuntion[14]. A homozygous 2-basepair (bp) deletion (c.422_423delAG) in *HSD17B4* results in a frameshift at amino acid (aa) 140, resulting in a truncated protein due to a premature stop codon[15]. The G16S missense mutation (c.46G > A), the most common cause of *HSD17B4* deficiency (type III), abolishes 3-hydroxyacyl-CoA dehydrogenase activity of HSD17B4[14]. In addition, the N457Y missense mutation (c.1369A > T), the second most common variant (type II), disrupts the enoyl-CoA hydratase domain[16]. Clinically, patients with *HSD17B4* deficiency manifest as early-onset hypotonia, seizures, craniofacial dysmorphism, severe neurodevelopmental impairment, cerebellar atrophy, and progressive loss of hearing and vision[14,17–19]. Notably, knockout (KO) mice for *Hsd17B4* exhibit phenotypic parallels, including growth retardation, infertility, liver fibrosis, motor dysfunction with cerebellar atrophy, and visual deficits due to defective peroxisomal β-oxidation[20–23]. Strikingly, the clinical features of *HSD17B4* deficiency strongly resemble ciliopathy-like phenotypes caused by defects in primary cilia including developmental delay, abnormal fertility, liver fibrosis, and cerebellar atrophy[24–28]. Nevertheless, the possible correlation between *HSD17B4* deficiency and ciliopathy remains poorly understood, which prompted us to investigate the role of *HSD17B4* in primary ciliogenesis and its possible contribution to ciliopathy-like phenotypes. Therefore, in this study, we aimed to elucidate a potential functional connection between *HSD17B4* deficiency and ciliary dysregulation, providing mechanistic insight into ciliopathy-like features observed in *HSD17B4*-deficient models.

Results

Loss of *HSD17B4* triggers ciliopathy-like symptoms

Thus, we hypothesized that *HSD17B4* deficiency contributes to ciliary dysfunction and investigated the uncovered effect of *HSD17B4* deficiency on primary ciliogenesis. To assess primary cilia formation, patient-derived primary dermal fibroblasts carrying the *HSD17B4* c.422_423delAG mutation were examined using immunostaining for ADP-ribosylation factor-like protein 13B (ARL13B). Notably, *HSD17B4*-deficient fibroblasts exhibited significantly impaired ciliogenesis, as indicated by a reduced number of ciliated cells and shortened ciliary length compared to control fibroblasts (Fig. 1a–c). Consistently, primary ciliary dysgenesis was also observed in both *HSD17B4*-knockdown RPE cells and *HSD17B4*-knockout (KO) SH-SY5Y cells (Fig. 1d–g, Supplementary Fig. 1a–c). Given the role of primary cilia in transducing multiple signaling pathways, we further examined the impact of *HSD17B4* deficiency on primary cilia-mediated signaling. Loss of *HSD17B4* altered ciliary signaling, including Smad 2/3-mediated TGF-β and GLI2-mediated Sonic hedgehog (Shh) pathways (Fig. 1h, Supplementary Fig. 1d–g). These findings suggest that *HSD17B4* deficiency disrupts primary ciliogenesis and impairs cilia-dependent signaling pathways.

Dysregulation of peroxisomal β-oxidation impairs primary ciliogenesis leading to defective ciliary formation

To further investigate the role of HSD17B4 in primary ciliogenesis, we examined its impact under conditions that promote primary ciliogenesis. Notably, depletion of *HSD17B4* significantly suppressed primary ciliogenesis even following stimulation with known primary cilia stimulators, including serum deprivation, the Smoothened agonist (SAG), and GSK503 (Fig. 2a, b). Given that HSD17B4 is a critical enzyme in peroxisomal β-oxidation, which proceeds in four sequential reactions mediated by ABCD1 and ACOX1[10,29], we further explored whether perturbations in the peroxisomal β-oxidation pathway affect primary cilia formation. Strikingly, disruption of additional peroxisomal β-oxidation-related genes, including *ABCD1*, *ACOX1*, *TYSND1*, and *HSD17B4*, markedly impaired primary ciliogenesis under serum deprivation conditions (Fig. 2c, d). These findings indicate that dysregulation of peroxisomal β-oxidation caused by *HSD17B4* deficiency disrupts primary ciliogenesis, highlighting a previously unrecognized link between peroxisomal metabolism and ciliary dynamics.

Restoration of acetyl-CoA levels rescues primary cilia defects caused by *HSD17B4* mutations

Peroxisomal β-oxidation plays a crucial role in cellular metabolism by generating a substantial proportion of cellular metabolites through the degradation of fatty acids. To identify key metabolites involved in primary ciliogenesis in *HSD17B4*-deficient cells, we conducted a high-content, cell-based screening using a metabolite library containing ~550 compounds (Supplementary Fig. 2a, Supplementary Data 1). This screening revealed that several peroxisomal β-oxidation end-products, including acetyl-CoA, which is a central energy metabolic intermediate[30,31] effectively rescued ciliary dysgenesis in *HSD17B4*-depleted cells (Supplementary Fig. 2b). Notably, previous studies have demonstrated that the manipulation for acetyl-CoA synthesis and supplementation of acetate, a source of acetyl-CoA, can elevate intracellular acetyl-CoA levels and promote lipid synthesis[32–34]. Consistently, we confirmed the screening results and found that treatment with either acetyl-CoA or acetate efficiently restored primary ciliogenesis in *HSD17B4*-deficient cells (Supplementary Fig. 2c, d). To further investigate the role of acetyl-CoA in ciliogenesis, we assessed acetyl-CoA levels in *HSD17B4*-KO cells and found that they were significantly reduced in *HSD17B4*-KO cells (Supplementary Fig. 3a). To extend the findings to a disease-relevant context, we measured acetyl-CoA levels in patient-derived fibroblasts harboring the *HSD17B4* c.422_423delAG mutation and found a marked reduction compared with healthy control fibroblasts. Importantly, supplementation with acetate restored acetyl-CoA levels in patient-derived fibroblasts (Fig. 3a). Functionally, we found that acetate treatment significantly enhanced primary ciliogenesis in patient-derived fibroblasts and SH-SY5Y cells (Fig. 3b, c, Supplementary Fig. 3b–e). Conversely, down-regulation of acetyl-CoA synthetase 2 (ACSS2)—which catalyzes the conversion of acetate to acetyl-CoA—impaired primary ciliogenesis (Supplementary Fig. 4a–c), suggesting that the acetate-mediated restoration of acetyl-CoA levels reverses *HSD17B4* deficiency-induced ciliary dysfunction. Previous studies have identified several missense mutations in *HSD17B4* that result in the complete inactivation of its enzymatic activities, including the G16S mutation, which abolishes 3-hydroxyacyl-CoA dehydrogenase activity, and the N457Y mutation, which disrupts enoyl-CoA hydratase activity (Fig. 3d, e)[14,16]. Therefore, we further examined whether acetate could rescue ciliogenesis defects in cells expressing these loss-of-function *HSD17B4* mutants. While reconstitution with WT *HSD17B4* effectively restored primary ciliogenesis in *HSD17B4*-KO cells, the mutant forms (G16S and N457Y) failed to do so. However, consistent with our findings in patient-derived fibroblasts, acetate supplementation significantly enhanced ciliogenesis in both *HSD17B4* mutant- and WT- expressing cells (Fig. 3f, g). These results indicate that acetate supplementation rescues primary

https://doi.org/10.1038/s41467-025-57793-8

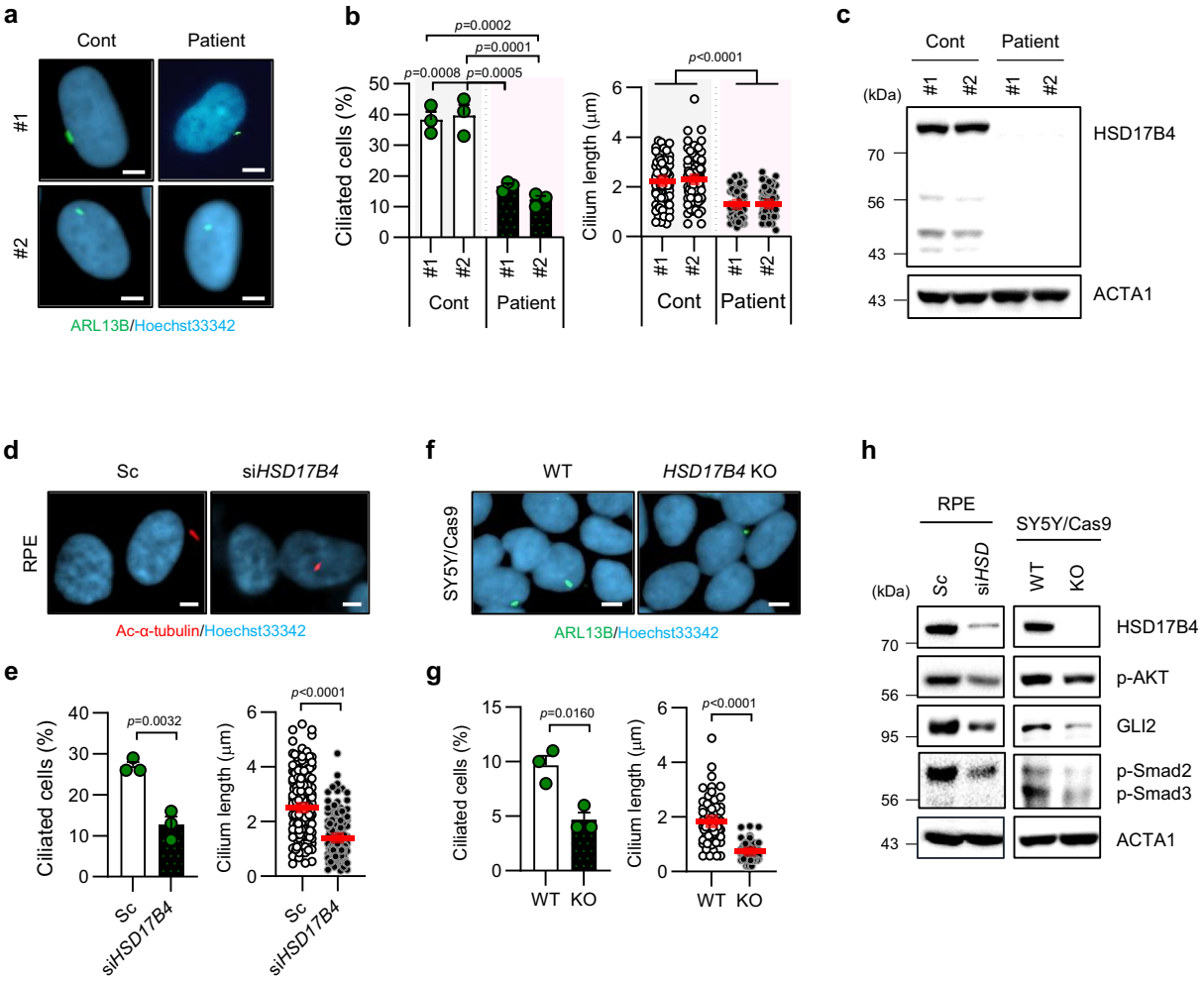

Fig. 1 | Loss of *HSD17B4* leads to dysgenesis of primary cilia in different cell types. a, **b** Primary cilia were visualized in fibroblasts derived from healthy controls (Cont #1, #2) and *HSD17B4*-deficient patients (c.422_423DelAG; Patient #1, #2) by immunostaining with an anti-ARL13B (green) antibody. Nuclei were counterstained with Hoechst 33342 dye (blue). Data are presented as the mean ± SEM (n = 3, independent biological replicates). *P*-value vs. healthy controls determined by one-way ANOVA followed by Tukey's multiple comparisons test [Ciliated cells: Cont #1 vs. Patient #1 $p = 0.0008$, vs. Patient #2 $p = 0.0002$; Cont #2 vs. Patient #1 $p = 0.0005$, vs. Patient #2 $p = 0.0001$; Cilium length: Cont #1, 2 vs. Patient #1, 2 $p < 0.0001$]. **c** HSD17B4 expression was abrogated in *HSD17B4* patient-derived fibroblasts. Western blot analysis was performed using the indicated antibodies. Representative blot from three independent experiments is presented **d**, **e** RPE cells were transfected with either scrambled (Sc) siRNA or siRNA targeting *HSD17B4* (si*HSD17B4*) for 72 h. Primary cilia were immunostained with an anti-acetylated-α-tubulin antibody (red), and nuclei were counterstained with Hoechst 33342 dye (blue). **f**, **g** *HSD17B4*-knockout (KO) and wild-type (WT) SH-SY5Y/Cas9 cells were immunostained with an anti-ARL13B (green) antibody and Hoechst 33342 (blue) dye. The number of ciliated cells and the ciliary length of the cells were quantified using a fluorescence microscope. Scale bar, 5 μm. Data are presented as the mean ± SEM (n = 3, independent biological replicates). *P*-value vs. Sc non-targeting siRNA treatment or WT cells determined by two-tailed unpaired *t*-test [Ciliated cells: Sc vs. si*HSD17B4* $p = 0.0032$ (**e**), WT vs. KO $p = 0.0160$ (**g**); Cilium length: Sc vs. si*HSD17B4*, WT vs. KO $p < 0.001$ (**e**, **g**)]. **h** Primary cilia-mediated signaling was assessed by western blotting using the indicated antibodies. Experiments were repeated three times. Source data are provided as a Source Data file.

cilia defects caused by *HSD17B4* deficiency, highlighting acetyl-CoA as a critical metabolite in primary ciliogenesis.

HDAC6 mediates acetyl-CoA-induced primary ciliogenesis in *HSD17B4*-deficient cells

Next, we investigated the molecular mechanism underlying the dysregulation of primary ciliogenesis induced by *HSD17B4* deficiency. Several remarkable studies have demonstrated that acetyl-CoA post-translationally regulates enzymatic activity by modulating protein acetylation[32–34]. Conversely, the deprivation of cellular acetate reduces intracellular acetyl-CoA levels, potentially affecting key regulatory pathways. To examine the impact of histone deacetylase (HDAC) activity on primary ciliogenesis, we treated *HSD17B4*-WT and -KO cells with various HDAC inhibitors (Fig. 4a–c, Supplementary Fig. 5a, b). Notably, primary ciliogenesis defects in *HSD17B4*-KO cells were markedly rescued by treatment with Tubastatin A, an HDAC6 selective inhibitor, as well as by pan-HDAC inhibitors such as TSA, VPA, and SAHA. These findings indicate that HDAC6 contributes to dysregulation of primary ciliogenesis in *HSD17B4*-deficient cells (Fig. 4b–d, Supplementary Fig. 5c–f). Consistent with this notion, previous studies have reported that the upregulation of HDAC6 leads to the deacetylation of α-tubulin, whereas HDAC6 inhibition strongly increases acetylated α-tubulin, thereby promoting primary ciliogenesis[4,35]. To further validate the role of HDAC6 in primary ciliogenesis, we examined the effect of HDAC6 deletion in *HSD17B4*-deficient mouse embryonic fibroblasts (MEFs). Strikingly, the ciliogenesis defects caused by *HSD17B4* deficiency were almost completely rescued upon *HDAC6* deletion, accompanied by a significant increase in α-tubulin acetylation (Fig. 4e–g). Collectively, these findings suggest that HDAC6 mediates ciliary dysgenesis in *HSD17B4*-deficient cells by suppressing α-tubulin acetylation in response to decreased acetyl-CoA levels.

https://doi.org/10.1038/s41467-025-57793-8

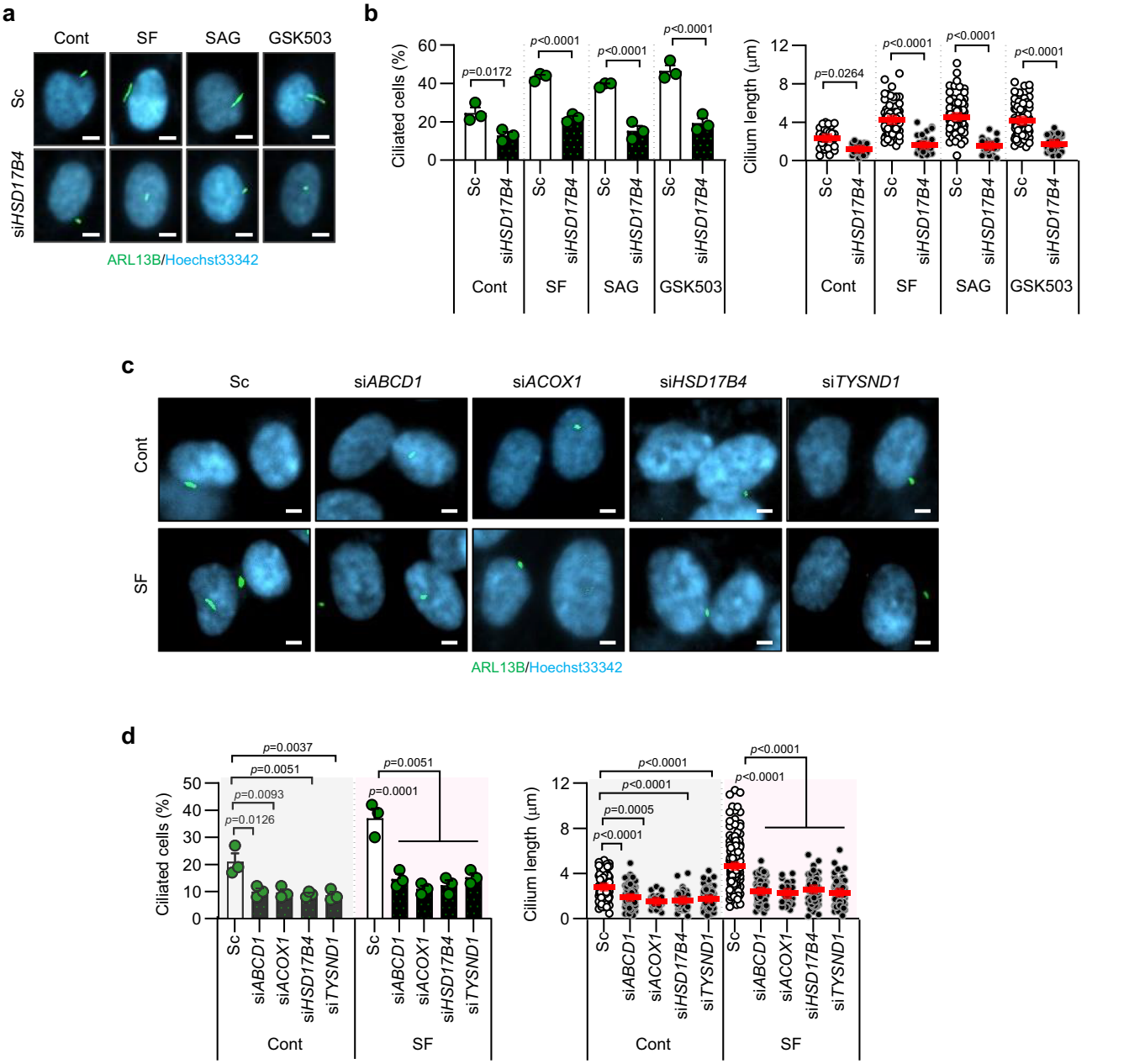

Fig. 2 | Impairment of the peroxisomal β-oxidation pathway disrupts primary ciliogenesis in RPE cells. a, **b** The RPE cells were transfected with a Sc or an *HSD17B4* siRNA (si*HSD17B4*). After incubation for 48 h, the cells were treated with serum-free (SF) medium, SAG (1 μM), or GSK503 (10 μM) for 24 h. Primary cilia were immunostained with an anti-ARL13B antibody (green) and the nuclei were counterstained with Hoechst 33342 dye (blue). Data are presented as the mean ± SEM (n = 3, independent biological replicates). *P*-value vs. between the indicated groups determined by one-way ANOVA followed by Tukey's multiple comparisons test [Ciliated cells: Sc vs. si*HSD17B4*; Cont $p = 0.0172$, SF $p < 0.0001$, SAG $p < 0.0001$, GSK503 $p < 0.0001$; Cilium length: Sc vs. si*HSD17B4*; Cont $p = 0.0264$, SF, SAG, and GSK503 $p < 0.001$]. **c**, **d** The RPE cells transfected with the indicated siRNA for the dysregulation of peroxisomal β-oxidation pathway were further incubated with or w/o SF medium. The primary cilia were immunostained with anti-ARL13B (green) antibody, and the nuclei were counterstained with Hoechst 33342 dye (blue). Data are presented as the mean ± SEM (n = 3, independent biological replicates). *P*-value vs. between the indicated groups determined by one-way ANOVA followed by Tukey's multiple comparisons test [Ciliated cells: Cont Sc vs. si*ABCD1* $p = 0.0126$, si*ACOX1* $p = 0.0093$, si*HSD17B4* $p = 0.0051$, si*TYSND1* $p = 0.0037$; SF Sc vs. si*ABCD1*, si*ACOX1*, si*HSD17B4*, si*TYSND1* $p = 0.0051$; Cilium length: Cont Sc vs. si*ABCD1* $p < 0.0001$, si*ACOX1* $p = 0.0005$, si*HSD17B4* $p < 0.0001$, si*TYSND1* $p < 0.0001$; SF Sc vs. si*ABCD1*, si*ACOX1*, si*HSD17B4*, si*TYSND1* $p < 0.001$]. Scale bar, 5 μm. Source data are provided as a Source Data file.

Genetic ablation of *Hsd17B4* causes ciliopathy-like pathological features in mice

As we found that the depletion of *HSD17B4* is associated with dysregulated primary ciliogenesis, we further investigated the relationship between *Hsd17B4* deficiency and ciliopathy development in an in vivo mouse model. *Hsd17B4*-knockout (*Hsd17B4*$^{-/-}$) mice exhibited a complete loss of *Hsd17B4* expression in major organs, including the liver, kidney, lung, brain, and heart, compared with wild-type (*Hsd17B4*$^{+/+}$) controls (Fig. 5a). In parallel with the expression deficit, the *Hsd17B4*$^{-/-}$ mice displayed severe growth retardation from an early stage and exhibited a significantly higher mortality rate (Fig. 5b, c). The average body weight of *Hsd17B4*$^{-/-}$ mice was markedly lower than that of *Hsd17B4*$^{+/+}$ mice, with a progressive decline beginning at 9 weeks or age (Fig. 5b, Supplementary Fig. 6a). Moreover, survival rates began to decline at 3 weeks, dropping to <30% by 12 weeks, with only a few mice surviving beyond 13 weeks (Fig. 5c). Histological analysis of the kidney

https://doi.org/10.1038/s41467-025-57793-8

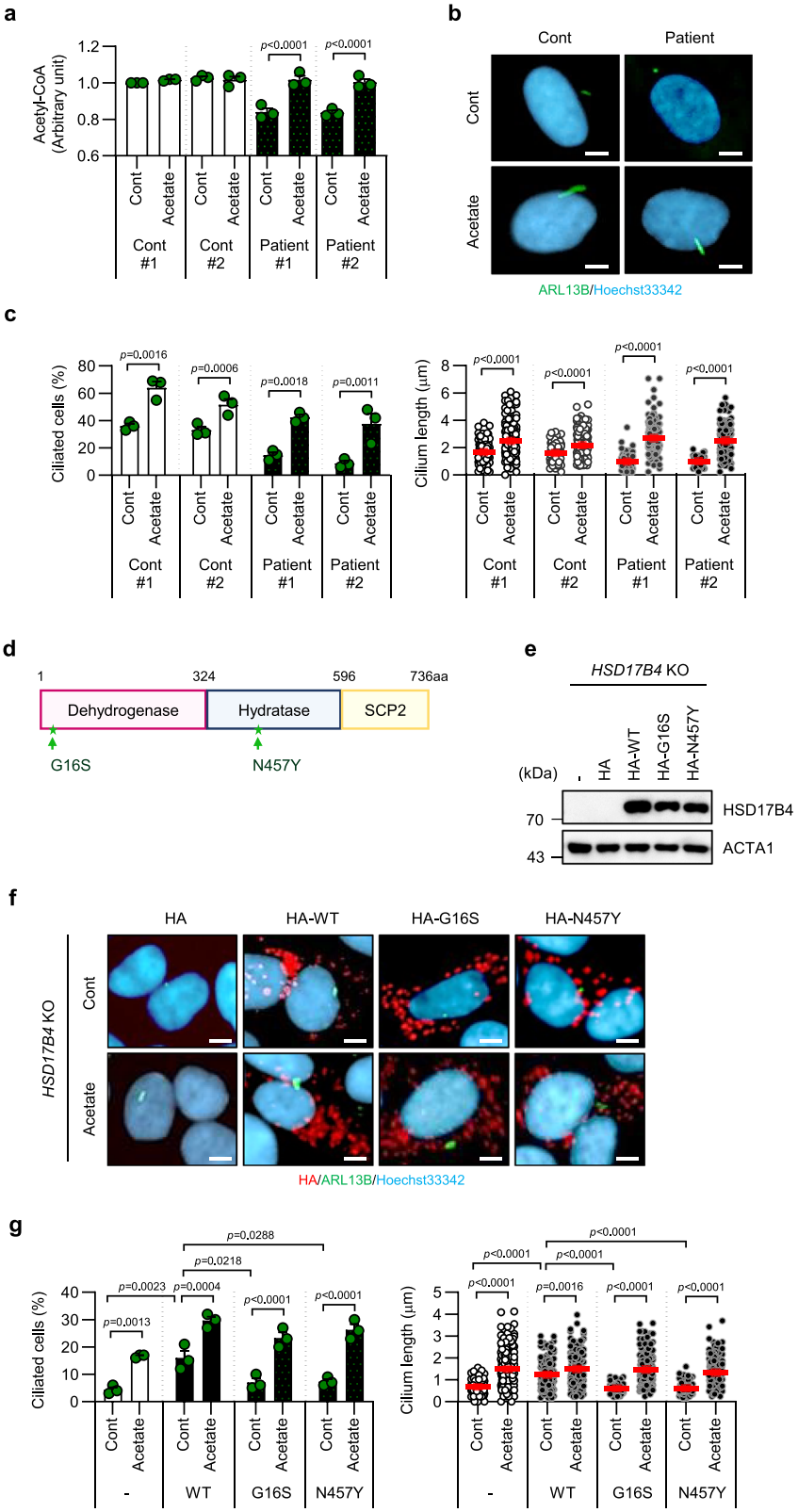

and liver of aged *Hsd17B4*$^{-/-}$ mice revealed fibrosis, a characteristic feature of ciliary dysfunction, compared with *Hsd17B4*$^{+/+}$ controls (Supplementary Fig. 6b, c). Notably, brain histology in *Hsd17B4*$^{-/-}$ mice revealed irregular cerebellar lobule development, a significantly reduced cerebellar size, and marked decrease in the number of Purkinje cells, along with thinning of the molecular layer (Fig. 5d, e). These morphological abnormalities were associated with distinct behavioral impairments. Specifically, *Hsd17B4*$^{-/-}$ mice exhibited motor coordination deficits, as assessed by the rota-rod test, at 9 weeks of age, in contrast to the preserved motor function observed in *Hsd17B4*$^{+/+}$ mice (Fig. 5f). This motor dysfunction is likely attributable to the loss of Purkinje cells in the cerebellum of *Hsd17B4*$^{-/-}$ mice, along with the significant reduction in primary ciliogenesis observed in these mice (Fig. 5g–k). Collectively, these findings demonstrate that *Hsd17B4*

Fig. 3 | Acetate supplementation restores primary ciliogenesis disrupted by *HSD17B4* mutations. a–c Fibroblasts derived from healthy controls (Cont #1, Cont #2) and *HSD17B4*-deficient patients (422_423DelAG; Patient #1, #2) were treated with sodium acetate (10 mM) for 24 h. **a** Intracellular acetyl-CoA levels were assessed using an acetyl-CoA ELISA kit from whole-cell lysates. Representative data from three independent experiments (n = 3) are presented as the mean ± SEM. [Patient #1, #2: Cont vs. Acetate $p < 0.001$]. **b**, **c** Primary cilia were immunostained with an anti-ARL13B (green) antibody, and the nuclei were counterstained with Hoechst 33342 (blue) dye. Data are presented as the mean ± SEM (n = 3, independent biological replicates). [Ciliated cells: Cont vs. Acetate; Cont #1 $p = 0.0016$, Cont #2 $p = 0.0006$, Patient #1 $p = 0.0018$, Patient #2 $p = 0.0011$; Cilium length: Cont vs. Acetate; Cont #1, 2, Patient #1, 2 $p < 0.001$]. **d** Schematic representation of HSD17B4 domains: dehydrogenase (pink), hydratase (blue), and SCP2 (yellow). The patient-derived mutations (G16S and N457Y) are indicated. **e–g** SY5Y/Cas9 *HSD17B4*-KO cells were transfected with hemagglutinin (HA)-tagged WT or mutant (G16S or N457Y) *HSD17B4* constructs. **e** The expression of HSD17B4 was examined by western blotting. Representative blot from three independent experiments is shown. **f**, **g** *HSD17B4* WT or mutant-overexpressing SY5Y/Cas9 *HSD17B4*-KO cells were co-stained with an anti-HA (red), anti-ARL13B (green) for primary cilia, and Hoechst 33342 (blue) for nuclei. Data are presented as the mean ± SEM (n = 3, independent biological replicates). [Ciliated cells: Cont vs. Acetate; Cont $p = 0.0013$, WT $p = 0.0004$, G16S $p < 0.0001$, N457Y $p < 0.0001$; Cilium length: Cont vs. Acetate; Cont $p < 0.0001$, WT $p = 0.0016$, G16S $p < 0.0001$, N457Y $p < 0.0001$]. *P*-value vs. between the indicated groups determined by one-way ANOVA followed by Tukey's multiple comparisons test. Scale bar, 5 µm. Source data are provided as a Source Data file.

deficiency leads to growth retardation and motor dysfunction in association with primary cilia dysregulation.

Acetate administration rescues the ciliopathy-like defects in *Hsd17B4*-deficient mice

The cerebellum serves as a key regulator of motor functions, including voluntary movement coordination and motor learning, while also contributing to certain cognitive and emotional processes[36,37]. Structurally, the cerebellum is divided into anterior and posterior lobes, with the anterior lobe and the lobule IV/V specifically implicated in motor and social processes. To determine whether acetate administration could mitigate the neurological defects associated with *Hsd17B4* deficiency, acetate was administered to mice both during and after gestation, followed by phenotypic analysis. Although acetate administration did not alter birth rates (Fig. 6a), it significantly improved survival in *Hsd17B4*$^{-/-}$ mice. In the untreated *Hsd17B4*$^{-/-}$ group, survival rates were ~30%, whereas acetate-treated *Hsd17B4*$^{-/-}$ mice exhibited a significantly increased survival rate of nearly 70% (Fig. 6b). Furthermore, histological analysis of acetate-treated *Hsd17B4*$^{-/-}$ mice revealed a marked increase in cerebellar size and restoration of lobular morphology (Fig. 6c). Functionally, acetate treatment substantially improved motor coordination in *Hsd17B4*$^{-/-}$ mice (Fig. 6d). Moreover, *Hsd17B4* deficiency resulted in degenerative cerebellar phenotypes, characterized by the loss and malformation of Purkinje cells in lobule IV/V, which likely contributed to motor coordination deficits. Notably, acetate administration significantly restored the loss of Purkinje cells in lobule IV/V and repaired the structural morphology compared with untreated *Hsd17B4*$^{-/-}$ mice (Fig. 6e). These morphological improvements correlated with enhanced primary ciliogenesis in the cerebellum. Consistently, in addition to increased survival rates, acetate-treated *Hsd17B4*$^{-/-}$ mice exhibited a significant restoration of primary ciliogenesis compared with untreated *Hsd17B4*$^{-/-}$ controls (Fig. 6f–i, Supplementary Fig. 7). Moreover, key signaling factors regulated by primary cilia were remarkably restored in the cerebellum following acetate administration (Fig. 6j, k). Similarly, administration of Tubastatin A, a selective HDAC6 inhibitor, in *Hsd17B4*$^{-/-}$ mice produced comparable effects, including improved motor function, mitigation of cerebellar deficits, enhanced primary ciliogenesis, and restoration of Purkinje cell layer within lobule IV/V (Supplementary Fig. 8). These findings collectively indicate that acetate administration rescues ciliopathy-like phenotypes in *Hsd17B4*-deficient mice by restoring primary ciliogenesis and cerebellar function.

Discussion

In cooperation with mitochondria, peroxisomes play a critical role in lipid metabolism through peroxisomal β-oxidation[38,39]. Notably, the accumulation of VLCFAs and the impaired fatty acid β-oxidation via peroxisomal dysfunction have been implicated in various disorders, including peroxisome biogenesis disorder (PBD), which manifest as severe pathological symptoms such as early-onset lethality, deafness, vision loss, and brain developmental abnormalities[40–43]. However, the relationship between peroxisomes and primary cilia has not been established. In this study, we identified a possible link between peroxisomal function and primary ciliogenesis. Specifically, *HSD17B4* abrogation led to defective primary ciliogenesis across multiple *HSD17B4*-inhibited models, including patient-derived fibroblasts harboring *HSD17B4* mutations, *HSD17B4* knockdown cells, and *HSD17B4*-KO cells (Fig. 1). Furthermore, loss of *HSD17B4* disrupted primary cilia-associated signaling pathways (Fig. 1, Supplementary Fig. 1). Consistently, knockdown of key peroxisomal β-oxidation enzymes, including *ABCD1*, *ACOX1*, and *TYSND1*, similarly impaired primary ciliogenesis (Fig. 2). Importantly, we observed that treatment with known primary cilia inducers, such as Smoothened agonist (SAG) and GSK503 (an EZH2 inhibitor), failed to restore primary ciliogenesis in *HSD17B4*-deficient cells (Fig. 2). However, metabolic analysis revealed that *HSD17B4* inhibition fundamentally downregulated intracellular acetyl-CoA levels. Notably, sodium acetate supplementation rescued primary ciliary dysgenesis by restoring acetyl-CoA levels in *HSD17B4*-deficient cells (Fig. 3, Supplementary Fig. 3). Furthermore, reconstitution with wild-type (WT) *HSD17B4* successfully restored primary ciliogenesis in *HSD17B4*-KO cells (Fig. 3). In contrast, overexpression of missense mutants of *HSD17B4* (G16S, N457Y) failed to rescue ciliogenesis defects, indicating that these mutations impair *HSD17B4*-dependent peroxisomal β-oxidation, which is critical for proper ciliogenesis (Fig. 3). Collectively, our findings implicate peroxisomal β-oxidation as a key metabolic pathway regulating primary ciliogenesis. Given the insights, further investigations are warranted to understand the precise molecular mechanisms involved in the regulation of primary ciliogenesis through peroxisomal β-oxidation.

Acetyl-CoA is well established as a key regulator of histone acetylation, modulating gene expression through the activity of histone acetyltransferases (HATs) and histone deacetylases (HDACs)[44,45]. HDAC6, a class IIb HDAC, specifically promotes α-tubulin deacetylation, leading to destabilization of the primary ciliary axoneme and subsequent ciliary disassembly[4,35]. Accordingly, genetic or pharmacological inhibition of HDAC6 prevents ciliary disassembly, and enhances primary ciliogenesis[46]. Consistently, we observed that HDAC6 inhibition significantly rescued primary ciliogenesis defects in *HSD17B4*-KO cells. Furthermore, the dysregulation of primary ciliogenesis triggered by *HSD17B4* deficiency was effectively restored in *HDAC6*-deficient cells (Fig. 4, Supplementary Fig. 5).

Previous studies by the Baes group demonstrated that *Hsd17B4* deletion leads to growth retardation, infertility, testicular degeneration, and neurodegeneration, which are common hallmarks of ciliopathy[20,21,42,43]. In agreement with these findings, we observed that *Hsd17B4*$^{-/-}$ mice exhibited renal and hepatic fibrosis, along with impaired motor coordination and Purkinje cell malformation associated with disrupted primary ciliogenesis (Fig. 5, Supplementary Fig. 6). Given that primary cilia are essential for the connectivity and survival of cerebellar Purkinje neurons, *Hsd17B4* deficiency may contribute to ciliogenesis defects by disrupting metabolic homeostasis[7,47,48]. Acetyl-CoA plays a central role in cellular energy metabolism, including its involvement in

https://doi.org/10.1038/s41467-025-57793-8

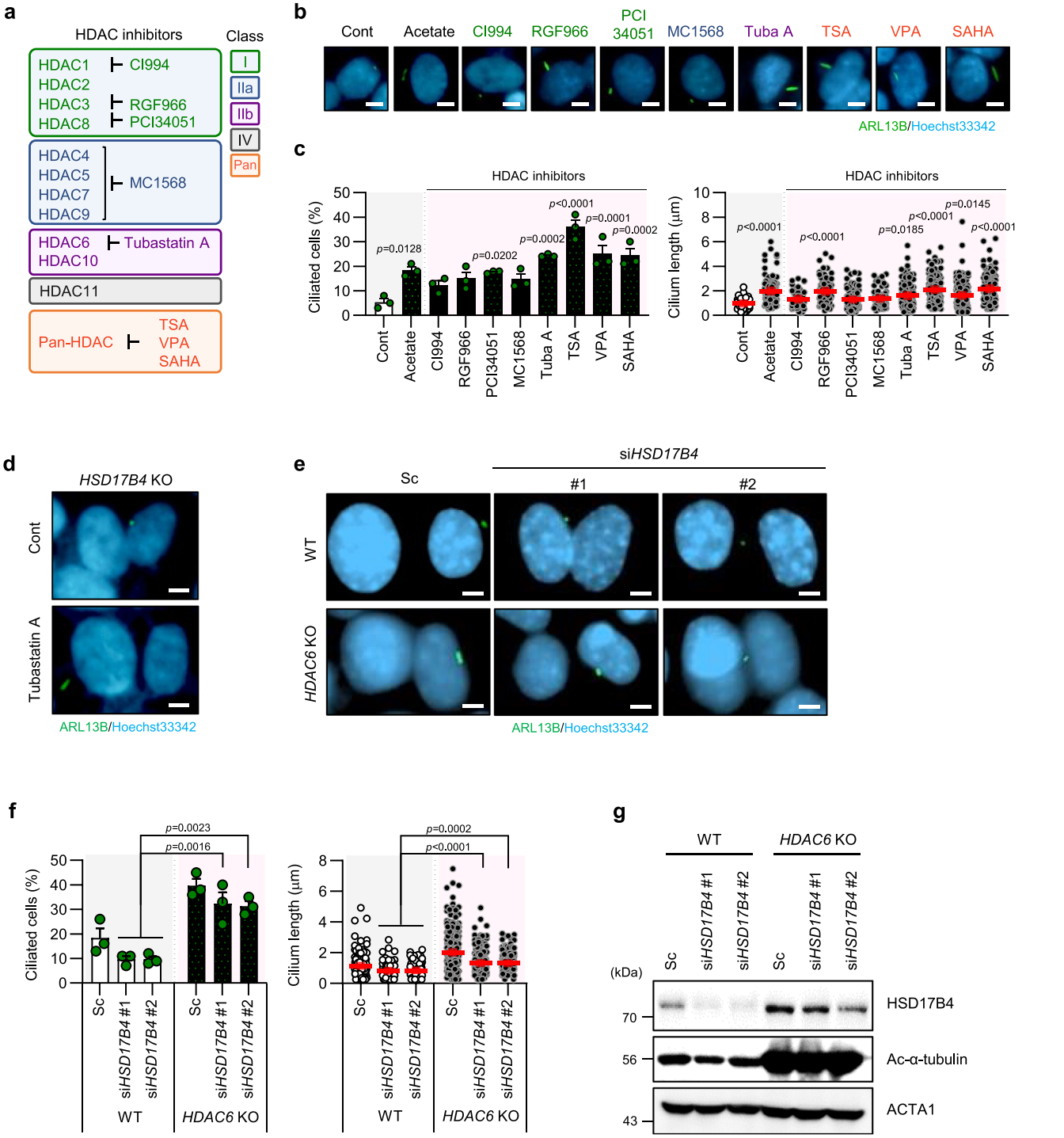

Fig. 4 | HDAC6 mediates acetyl-CoA-induced ciliogenesis in *HSD17B4*-deficient cells. a Schematic diagram of HDAC inhibitors. HDAC inhibitors were categorized into classes I, IIa, IIb, and IV, with each HDAC inhibitor targeting a different class of HDAC. **b**–**d** *HSD17B4*-KO SY5Y/Cas9 cells were separately treated with the indicated HDAC inhibitors for 24 h. The cells were immunostained with an anti-ARL13B (green) antibody and Hoechst 33342 (blue) dye. Data are presented as the mean ± SEM (n = 3, independent biological replicates). *P*-value vs. treatment determined by one-way ANOVA followed by Tukey's multiple comparisons test [Ciliated cells: Cont vs. Acetate $p = 0.0128$, PIC34051 $p = 0.0202$, Tubastatin A (Tuba A) $p = 0.0002$, TSA $p < 0.0001$, VPA $p = 0.0001$, SAHA $p = 0.0002$; Cilium length: Cont vs. Acetate, RGF966, TSA, SAHA $p < 0.0001$, Tuba A $p = 0.0185$, VPA $p = 0.0145$]. **e**–**g** The *HDAC6*-WT or -KO MEFs were transiently transfected with a Sc or si*HSD17B4* (#1, #2) for 72 h. **e**, **f** The primary cilia were immunostained with an anti-ARL13B (green) antibody and the nuclei were counterstained with Hoechst 33342 (blue) dye. Data are presented as the mean ± SEM (n = 3, independent biological replicates). *P*-value vs. indicated groups determined by one-way ANOVA followed by Tukey's multiple comparisons test [Ciliated cells: WT vs. *HDAC6*-KO; si*HSD17B4* #1 $p = 0.0016$, si*HSD17B4* #2 $p = 0.0023$; Cilium length: WT vs. *HDAC6*-KO; si*HSD17B4* #1 $p < 0.0001$, si*HSD17B4* #2 $p < 0.0002$]. Scale bar, 5 μm. **g** The upregulation of acetylated α-tubulin (Ac-α-tubulin) was assessed by western blotting analysis using the indicated antibody. Representative blot from three independent experiments is presented. Source data are provided as a Source Data file.

https://doi.org/10.1038/s41467-025-57793-8

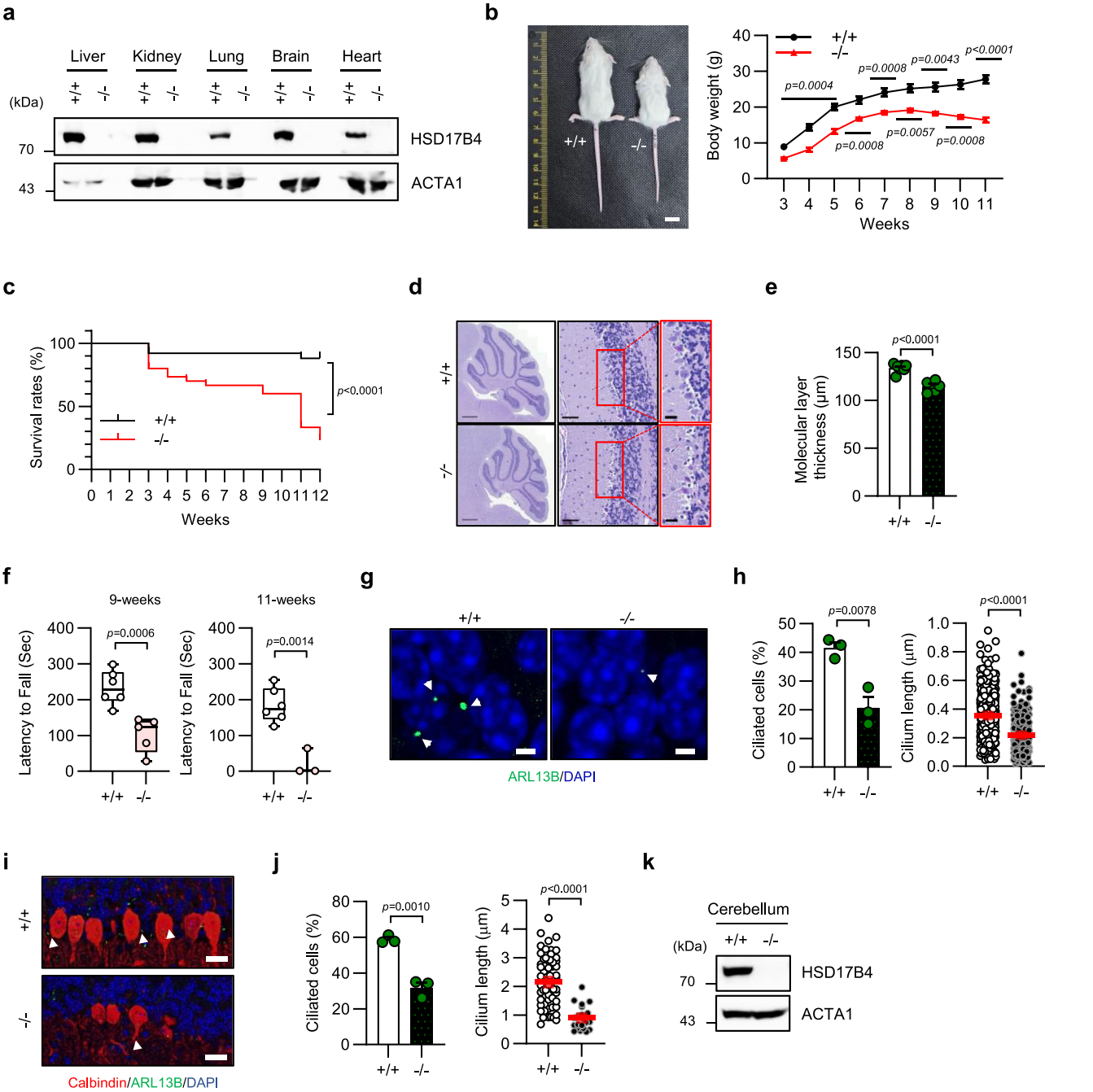

Fig. 5 | *Hsd17B4*-deficient mice exhibit a ciliopathy-like pathology. a Western blot analysis confirmed the downregulation of Hsd17B4 in *Hsd17B4*$^{-/-}$ mice (n = 3). **b** Growth retardation was assessed by imaging 11-week-old mice and measuring body weight from 3-week-old mice (*Hsd17B4*$^{+/+}$ n = 9; *Hsd17B4*$^{-/-}$ n = 7). Data are presented as the mean ± SEM. Statistical analysis was performed using two-way ANOVA with multiple comparisons. Scale bars, 1 cm. **c** Kaplan-Meier survival curves comparing *Hsd17B4*$^{+/+}$ (n = 25) and *Hsd17B4*$^{-/-}$ mice (n = 30) were analyzed using the Log-rank (Mantel-Cox) tests ($p < 0.0001$). **d** Representative images (n = 3) of H&E staining revealed reduced cerebellar volume, malformed lobules, and thinner molecular layers in *Hsd17B4*$^{-/-}$ mice. Scale bars, 500, 50, and 20 µm. **e** Molecular layer thickness was quantified in *Hsd17B4*$^{+/+}$ (n = 7) and *Hsd17B4*$^{-/-}$ (n = 6) mice ($p < 0.0001$). Data are presented as the mean ± SEM. **f** Motor function was evaluated using the rota-rod test in 9- and 11-week-old mice. Box plots represent the interquartile range (25th–75th percentile), median (central line), and minimum/maximum values (whiskers) [9-week-old *Hsd17B4*$^{+/+}$ (n = 6) Min = 59, Max = 300, Median = 280.5; *Hsd17B4*$^{-/-}$ (n = 5) Min = 18, Max = 190, Median = 105; 11-week-old *Hsd17B4*$^{+/+}$(n = 6) Min = 24, Max = 300, Median = 196; *Hsd17B4*$^{-/-}$ (n = 3) Min = 1, Max = 131, Median = 1]. [*Hsd17B4*$^{+/+}$ vs. *Hsd17B4*$^{-/-}$; 9 weeks $p = 0.0006$, 11 weeks $p = 0.0014$]. **g–j**. Immunofluorescence staining for primary cilia (ARL13B, green, white arrow; DAPI, blue) was performed in granular (Scale bar, 2 µm) and Purkinje (Scale bar, 20 µm) layers. Purkinje cells were counterstained with anti-calbindin (red). Data are presented as mean ± SEM (n = 3, independent biological replicates). [*Hsd17B4*$^{+/+}$ vs. *Hsd17B4*$^{-/-}$ Ciliated cells: $p = 0.0078$ (**h**), $p = 0.0010$ (**j**); Cilium length: $p < 0.0001$ (**h**, **j**)]. Statistical analysis was performed using a two-tailed unpaired *t*-test (**e–j**). **k** Western blot confirmed HSD17B4 expression in the cerebellum from three independent experiments. Source data are provided in the Source Data file.

https://doi.org/10.1038/s41467-025-57793-8

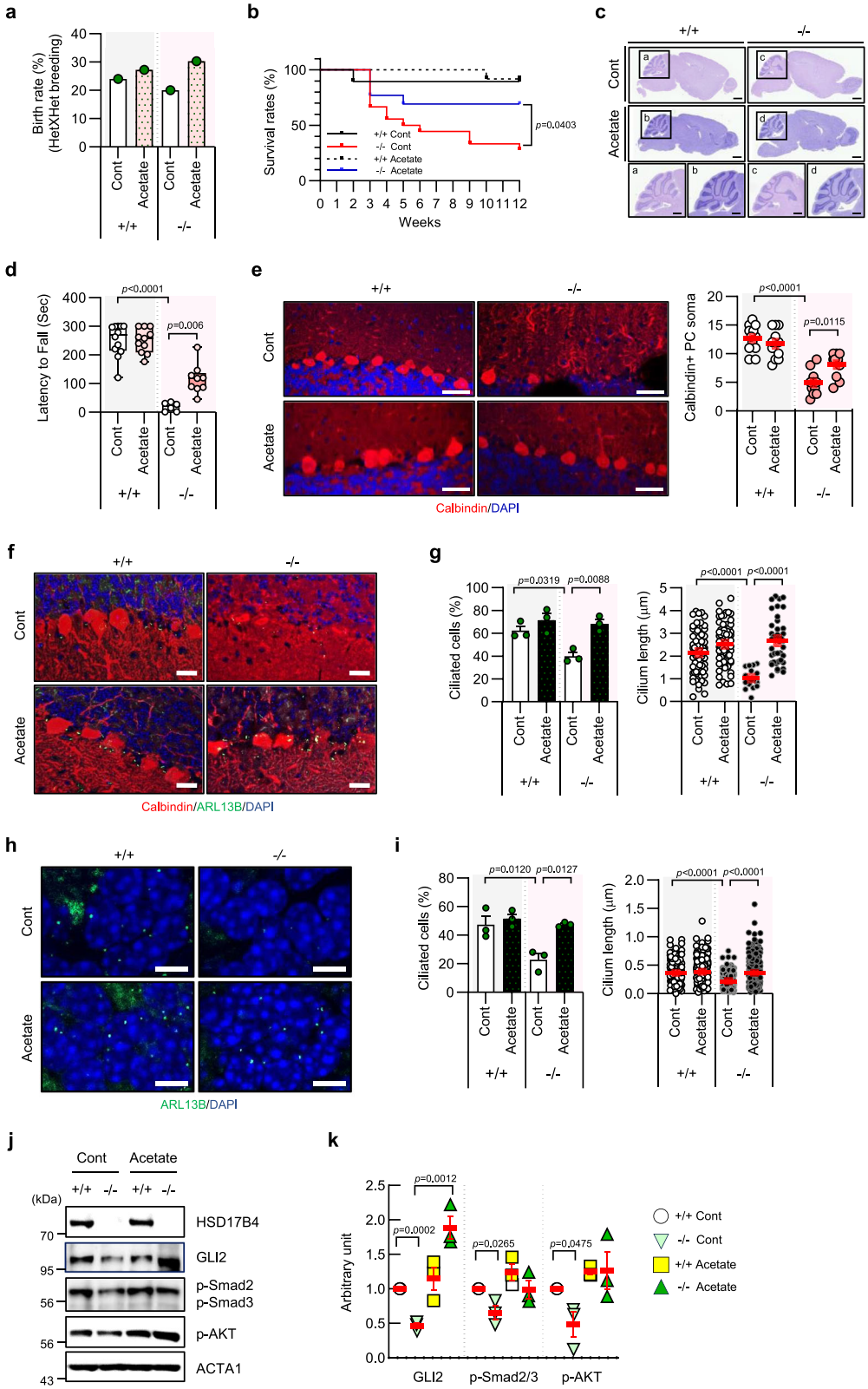

the tricarboxylic acid (TCA) cycle. As acetate is a metabolic precursor of acetyl-CoA, we hypothesized that acetate administration during development could alleviate the phenotypic defects associated with *Hsd17B4* deficiency by compensating for impaired peroxisomal β-oxidation (Fig. 6, Supplementary Fig. 7). In support of this hypothesis, we observed that acetate administration via drinking water effectively restored primary ciliogenesis and its associated signaling pathways in the cerebellum of *Hsd17B4*$^{-/-}$ mice (Fig. 6, Supplementary Fig. 7). Specifically, acetate administration increased the number of cerebellar Purkinje cells and improved structural integrity, mitigating the morphological abnormalities observed in *Hsd17B4*$^{-/-}$ mice. During development, Sonic hedgehog (Shh) signaling in Purkinje cells regulates the proliferation of granule cell precursors (GCP)[47,48]. Therefore, restoration of the Purkinje layer via acetate administration may contribute to the recovery of cerebellar lobules of the brain. More importantly, we found that severe motor dysfunction in *Hsd17B4*$^{-/-}$ mice was significantly

Fig. 6 | Acetate administration rescues ciliopathy-like phenotypes in *Hsd17B4*-deficient mice. a Birth rates of *Hsd17B4*$^{+/+}$ and *Hsd17B4*$^{-/-}$ mice were assessed with and w/o acetate administration (Cont n = 108; Acetate n = 57). **b** Survival rates were monitored for up to 12 weeks, showing a significant improvement in acetate-supplemented *Hsd17B4*$^{-/-}$ mice (n = 13) compared to untreated mice (n = 18). Kaplan-Meier survival curves were analyzed using the Log-rank (Mantel-Cox) test (*Hsd17B4*$^{+/+}$; Cont n = 19, Acetate n = 12; $p = 0.0403$). **c** H&E staining revealed reduced cerebellar volume and malformed lobules in *Hsd17B4*$^{-/-}$ mice. **d** Motor function was evaluated using the rota-rod test in 11-week-old mice. Acetate-treated *Hsd17B4*$^{-/-}$ mice exhibited improved performance compared to untreated mice. Box plots represent the interquartile range (25th–75th percentile), median (line), and minimum/maximum values (whisker) [*Hsd17B4*$^{+/+}$: Cont (n = 12) Min = 38, Max = 300, Median = 294; Acetate (n = 11) Min = 100, Max = 300, Median = 298; *Hsd17B4*$^{-/-}$: Cont (n = 6) Min = 1, Max = 41, Median = 21; Acetate (n = 9) Min = 37, Max = 288, Median = 109]. [*Hsd17B4*$^{+/+}$ vs. *Hsd17B4*$^{-/-}$ $p < 0.0001$; *Hsd17B4*$^{-/-}$ Cont vs. Acetate $p = 0.006$]. **e** Purkinje cell dysplasia in cerebellar lobule IV/V of *Hsd17B4*$^{-/-}$ mice was significantly improved by acetate administration (calbindin, red; DAPI, blue; Scale bar, 50 μm) [*Hsd17B4*$^{+/+}$ vs. *Hsd17B4*$^{-/-}$ $p < 0.0001$; *Hsd17B4*$^{-/-}$ Cont vs. Acetate $p = 0.0115$]. **f**–**i** Immunostaining of primary cilia in Purkinje and granular cells (calbindin, red; ARL13B, green; DAPI, blue) showed increased ciliary formation and elongation following acetate treatment [Ciliated cells: *Hsd17B4*$^{+/+}$ vs. *Hsd17B4*$^{-/-}$ $p = 0.0319$ (**g**), $p = 0.0120$ (**i**); *Hsd17B4*$^{-/-}$ Cont vs. Acetate $p = 0.0088$ (**g**), $p = 0.0127$ (**i**); Cilium length: *Hsd17B4*$^{+/+}$ vs. *Hsd17B4*$^{-/-}$ $p < 0.0001$ (**g**, **i**); *Hsd17B4*$^{-/-}$ Cont vs. Acetate $p < 0.0001$ (**g**, **i**)]. Scale bar, 20 μm. **j**, **k** Western blot analysis of primary cilia-mediated signaling [*Hsd17B4*$^{+/+}$ vs. *Hsd17B4*$^{-/-}$; GLI2 $p = 0.0002$, p-Smad2/3 $p = 0.0265$, p-AKT $p = 0.0475$; *Hsd17B4*$^{-/-}$ Cont vs. Acetate; GLI2 $p = 0.0012$]. Statistical analysis was performed using one-way ANOVA followed by Tukey's multiple comparisons test (**d**–**k**). Data are presented as mean ± SEM (n = 3, independent biological replicates). Source data are provided in the Source Data file.

improved following acetate administration (Fig. 6), further supporting the role of acetyl-CoA metabolism in ciliogenesis and neurological function.

Although our findings demonstrate that acetate treatment significantly enhances primary ciliogenesis by promoting tubulin acetylation, additional factors may contribute to this process. Recent studies suggest that tubulin palmitoylation may also play a role, particularly given that acetyl-CoA serves as a precursor for palmitate synthesis[49]. Furthermore, evidence indicate that inhibition of fatty acid synthesis may promote cilia restoration under certain conditions[50], potentially by redirecting acetyl-CoA utilization from lipid synthesis toward alternative cellular pathways. These findings highlight the need for further investigation to elucidate the mechanistic interplay between acetyl-CoA metabolism and ciliogenesis. Nevertheless, our study underscores the critical role of cellular acetyl-CoA levels in regulating primary ciliogenesis and suggests that targeting ciliogenesis defects may represent a promising therapeutic approach for *HSD17B4*-related diseases, including Perraut syndrome1. Although further preclinical and clinical investigations are required to validate these findings, our results provide a promising basis for exploring primary cilia restoration as a potential treatment strategy.

In conclusion, loss of *HSD17B4* is associated with a spectrum of diseases exhibiting ciliopathy-like phenotypes. Our findings suggest that restoration of acetyl-CoA levels through metabolic intervention may serve as a therapeutic strategy for *HSD17B4*-associated diseases.

Methods

Reagents

Acetyl coenzyme A sodium salt (acetyl-CoA, A2056), sodium acetate (S2889), Trichostatin A (T8552), and valproic acid (VPA, #1708707) were purchased from Sigma-Aldrich (St. Louis, MO, USA). Smoothened agonist (SAG, #566660) was purchased from Calbiochem (San Diego, CA, USA). GSK503 (HY-12856) was obtained from MedChem Express (Monmouth Junction, NJ). Suberoylanilide hydroxamic acid (SAHA) was provided by Crystal Genomics Co. (Seoul, South Korea). HDAC inhibitors, i.e., CI994 (S2818), RGF966 (S7229), PCI-34051 (S2012), MC1568 (S1484), and Tubastatin A (S8049), were purchased from Selleckchem (Houston, TX, USA). Hoechst 33342 (H3570) was obtained from Thermo Fisher Scientific (Waltham, MA, USA).

Cell lines

To generate the CRISPR/Cas9-mediated *HSD17B4*-KO cell lines, SH-SY5Y cells expressing CRISPR/Cas9 were co-transfected with crRNA targeting *HSD17B4* (Edit-R Human HSD17B4 (#3295) crRNA) and tracrRNA (Edit-R CRISPR-Cas9 Synthetic tracrRNA). The transfected individual cells were seeded into separate wells of 96-well plates, and single colonies with *HSD17B4* knockout (KO) were selected and validated. Fibroblasts (GM13263 and GM13264 cells) from human patients with *HSD17B4* deficiency (c.422_423DelAG) and healthy control fibroblasts (GM08333 and GM00969 cells) were obtained from Coriell Institute for Medical Research (Camden, NJ, USA). WT MEFs and *HDAC6* KO MEFs were generously provided by Dr. Joo-Yong Lee (GRAST, CNU, Daejeon, South Korea). Cells were maintained at 37 °C in a humidified 5% CO_2 incubator and cultured in Dulbecco's Modified Eagle's Medium (DMEM, WELGENE, Gyeongsan, Korea) containing 10% or 15% fetal bovine serum (FBS, WELGENE) and 1% penicillin-streptomycin (WELGENE).

Gene knockdown studies

Cells were transfected with validated small-inhibitory RNAs (siRNAs) targeting *ABCD1* (5′–GUUCAGCGCUGUCACUUCA–3′), *ACOX1* (5′–UUACAUGCCUUUAUCGUACUU–3′), *ACSS2* (5′-GGACCAGGAUGGCUAUUAC-3′), *HSD17B4* (5′–GGAAGAAGAUCUGUGACUUUU–3′), *TYSND1* (5′–CCCGCTGAGCACTTCCATGAA–3′), *IFT88* (5′–CCGAAGCACUUAACACUUA–3′), and mouse *HSD17B4* (#1, 5′–CAGUUGAAGCAGGCGAGAA–3′; #2, 5′–CAUUCAUUGCAACACCAUU–3′). The siRNAs were synthesized by Genolution (Seoul, South Korea).

Image-based metabolite library screening

For the screening of 550 metabolites, we utilized the Fecal Metabolites Library sourced from MetaSci Company (Catalog number: SKU_MSIFEC0001). This library comprises a comprehensive collection of fecal metabolites, including those indexed with a fecal origin in the Human Metabolome Database (HMDB) and metabolites found in the *E. coli* Metabolome Database (ECMDB). Additionally, it incorporates exogenous metabolites resulting from food consumption. A complete list of these metabolites is provided in the supplementary materials. htRPE/Smo-GFP (1×10^4) cells were seeded for image-based metabolite library screening (MetaSci, Toronto, ON, Canada) and the cells were treated with each metabolite and primary cilia were imaged under a fluorescence microscope (IX71, Olympus, Tokyo, Japan). Treatment with cytochalasin D (50 nM; C8273, Sigma-Aldrich), SAG (1 μM; #566661, Sigma-Aldrich), GSK503 (10 μM; HY-12856, MedChem Express), and serum deprivation was performed as positive controls for the induction of primary cilia by novel inducers. The experiments were repeated twice with consistent results.

Measurement of intracellular acetyl-CoA levels

SH-SY5Y/Cas9 *HSD17B4*-WT and -KO cell lines, fibroblasts from human patients with *HSD17B4* deficiency (c.422_423DelAG; GM13263 and GM13264), or healthy control fibroblasts (GM08333 and GM00969) were treated with either sodium acetate (10 mM; S2889, Sigma-Aldrich) or acetyl-CoA (100 μM; A2056, Sigma-Aldrich) for 24 h. Next, the levels of acetyl-CoA in the whole-cell lysates were measured using the acetyl-CoA assay kit (MAK039,

Sigma-Aldrich; ab87546, Abcam), as instructed by the manufacturer. Acetyl-CoA levels in liver samples from *Hsd17B4*$^{+/+}$ and *Hsd17B4*$^{-/-}$, following acetate treatment, were measured using a fluorometry-based assay (Sigma-Aldrich, MAK039). Liver tissues were processed according to the manufacturer's instructions. Processed samples were then incubated with the assay mix, which included acetyl-CoA substrates, conversion enzyme mix, and a fluorescent probe. After the reaction, fluorescence intensities were measured at an excitation wavelength of 535 nm and an emission wavelength of 587 nm (Synergy™ H1, BioTEK, Santa Clara, CA, USA).

Animals and recovery trial

The protocols used for all animal experiments were applied in accordance with the National Institutes of Health guidelines for the care and use of laboratory animals and were approved by the Committee for Handling and Use of Animals, Kyungpook National University (2021-0163). *Hsd17B4*-deleted mice, originally generated by Myriam Baes, were provided by the Katholieke Universiteit Leuven via the European Mouse Mutant Archive (EMMA). According to information provided by the supplier, the targeting vector for the removal of exons 1–3 of the *Hsd17b4* gene was transfected into R1 ES cells derived from a (129 × 1/SvJ × 129S1/Sv) F1 background. These ES cells were subsequently transferred to a Swiss background (SWR/OlaHsd) after being crossbred with Swiss animals. Sibling matings were then carried out for 35 generations. Male and female mice were housed in a controlled environment with temperature (21–23 °C), humidity (50–65%), and a 12:12 h light-dark cycle. They were provided standard chow (Altromin Mouse Diet, 1314) and water ad libitum. To investigate whether acetate treatment affected the retardation of *Hsd17B4*, we generated four groups of mice: *Hsd17B4*$^{+/+}$ and *Hsd17B4*$^{-/-}$ mice were assigned to two separate groups each based on whether they were provided water or 50 mM acetate (S2889, Sigma-Aldrich). The acetate solutions were administered instead of water to the female mice during and after pregnancy. Pups born from this group of mice were raised with sodium acetate until they were sacrificed for assessment. Both male and female mice were used in this study. *Hsd17B4*$^{+/+}$ and *Hsd17B4*$^{-/-}$ mice were administered a highly selective HDAC6 inhibitor Tubastatin A. Tubastatin A was dissolved in DMSO and then diluted with saline to a final concentration of 50 mg/kg/day. The solution was administered via daily intraperitoneal injections, starting at 9 weeks of age, which coincides with the onset of weight loss. The treatment was continued once daily for a 2-week period until the mice reached 11 weeks of age. The control group received the vehicle solution (DMSO diluted in saline) without Tubastatin A.

A rota-rod tests were performed on 9- and 11-week-old mice. The rotational speed was gradually increased from 4 to 40 rpm, and then maintained at 40 rpm for 5 min. Each mouse was allowed 10 min of rest before the next trial (BS technology RRMR). The latency to fall for each mouse was recorded over a total of four trials, including the training trial. A two-way repeated-measures analysis of variance (ANOVA) with mixed effects (with Tukey's post-hoc analysis) was performed to measure the improvement of motor functions following administration.

Immunostaining

For the immunostaining of primary cilia, the cells were fixed with 4% (w/v) paraformaldehyde (PFA) and permeabilized with 0.1% (v/v) Triton X-100. Following blocking, the cells were incubated overnight at 4 °C with primary antibodies against acetylated α-tubulin (1:3000, T7451, Sigma-Aldrich) or ARL13B (1:2000, 17711-1-AP, Proteintech, Chicago, IL). After washing, the cells were incubated with Alexa Fluor 488- or 555-conjugated secondary antibodies at room temperature (RT) for 1 h. The cilia images were acquired using a fluorescence or confocal microscope. Primary cilia were counted in ~200 cells under each experimental condition (n = 3). The percentage of ciliated cells was calculated as follows: (total number of cilia/total number of nuclei at each image) × 100. The length of primary cilia was measured in identified ciliated cells using the Free-hand Line Selection Tool of the Cell Sense Standards software (Olympus Europa Holding GmbH, Hamburg, Germany) for precise quantification, and the average ciliary length was calculated. The analysis of the graph data was performed using GraphPad Prism 10 (GraphPad Software, San Diego, CA). The mice were anesthetized and perfused with PBS. The harvested mouse tissue samples were embedded in paraffin, and the resulting sections were prepared and stained using standard histological techniques. Briefly, the paraffinized sections were deparaffinized in xylene, and then hydrated. The slides were then incubated overnight at 4 °C with the primary antibodies against ARL13B (1:1000, 75-287, NeuroMab) or Calbindin (1:1000, 13176S, Cell signaling), in 10% normal goat serum. Subsequently, the slides were incubated overnight at 4 °C with the appropriate secondary antibodies specific to the primary antibodies; Alexa Fluor 488- or Alexa Fluor 555-conjugated antibodies (1:1000, A-11001 or A-21428, Invitrogen). All slides were mounted with Fluoromount-G™ Mounting Medium (00-4958-02, Invitrogen). Images were acquired using a Super Resolution Confocal Laser Scanning Microscope (Carl Zeiss, LSM 800 with Airy Scan).

Western blotting

Cell lysates were prepared in 2X Laemmli sample buffer (Bio-Rad, Hercules, CA). After separation in 8%–12% SDS–PAGE, the proteins were transferred onto a PVDF membrane (Bio-Rad) and incubated with the following primary antibodies: anti-HSD17B4 (1:2000, ab128565, Abcam), anti-GLI2 (1:2000, 18989-1-AP, Proteintech), anti-phospho-AKT (S473) (1:1000, #9271, Cell Signaling Technology), anti-phospho-Smad2 (Ser465/467)/Smad3 (Ser423/425) (1:1000, #8828, Cell Signaling Technology), anti-acetylated α-tubulin (1:3000, T7451, Sigma-Aldrich), and anti-ACTA1 (1:10000, MAB1501, Millipore, Temecula, CA), anti-ACSS2 (1:3000, #3658S, Cell signaling). For protein detection, the membranes were incubated with horseradish peroxidase (HRP)-conjugated secondary antibodies (Pierce, Rockford, IL). Chemiluminescent signals were developed with the Western ECL substrate (WSE-7120L EzWestLumi plus, ATTO). Densitometry was performed on scanned immunoblots using the AE-9300 Ez-Capture MG Hours Image Saver HR image capture tool (ATTO, Tokyo, Japan). Protein expression levels in mice samples was normalized to that of actin. To extract the lysates, the harvested tissue samples of 9- or 11-week-old mice were immersed in the PRO-PREP™ Protein Extraction Solution (InTRON, Korea), homogenized using a tissue homogenizer, and sonicated. The extracted proteins were separated by 10% SDS–PAGE and transferred onto PVDF membranes (Millipore Sigma, Billerica, MA, USA). The membranes were incubated at 4 °C overnight with primary antibodies. After TBST washing, the membranes were incubated with anti-mouse (Cell Signaling Technology) or anti-rabbit (Cell Signaling Technology) secondary antibodies for 2 h at RT. The protein levels were detected using the Davinch-Chemi Chemiluminescence Imaging System (CoreBio, Seoul, Korea).

Statistical analysis

Statistical evaluation of the results was conducted using ANOVA followed by Tukey's multiple comparisons test or an unpaired two-tailed *t*-test, performed with GraphPad Prism 10 (GraphPad Software, San Diego, CA). Data were obtained from at least three independent experiments and are presented as mean ± standard error of the mean (SEM). P-values between the indicated groups were determined using ANOVA with Tukey's multiple comparisons test or an unpaired *t*-test. Statistical significance was set as $P < 0.05$ (n = 3), and the P-values are provided in the respective figures and figure legends.

Reporting summary

Further information on research design is available in the Nature Portfolio Reporting Summary linked to this article.

Data availability

All relevant data supporting the findings of this study are available within this article, its Supplementary Information and Source Data files. Source data are provided with this paper.

References

1. Goetz, S. C. & Anderson, K. V. The primary cilium: a signalling centre during vertebrate development. *Nat. Rev. Genet.* **11**, 331–344 (2010).
2. Anvarian, Z., Mykytyn, K., Mukhopadhyay, S., Pedersen, L. B. & Christensen, S. T. Cellular signalling by primary cilia in development, organ function and disease. *Nat. Rev. Nephrol.* **15**, 199–219 (2019).
3. Kiprilov, E. N. et al. Human embryonic stem cells in culture possess primary cilia with hedgehog signaling machinery. *J. Cell. Biol.* **180**, 897–904 (2008).
4. Hubbert, C. et al. HDAC6 is a microtubule-associated deacetylase. *Nature* **417**, 455–458 (2002).
5. Fliegauf, M., Benzing, T. & Omran, H. When cilia go bad: cilia defects and ciliopathies. *Nat. Rev. Mol. Cell. Biol.* **8**, 880–893 (2007).
6. Reiter, J. F. & Leroux, M. R. Genes and molecular pathways underpinning ciliopathies. *Nat. Rev. Mol. Cell. Biol.* **18**, 533–547 (2017).
7. Bowie, E. & Goetz, S. C. TTBK2 and primary cilia are essential for the connectivity and survival of cerebellar Purkinje neurons. *eLife* **9**, e51166 (2020).
8. Maharjan, Y. et al. TMEM135 regulates primary ciliogenesis through modulation of intracellular cholesterol distribution. *EMBO Rep.* **21**, e48901 (2020).
9. Miyamoto, T. et al. Insufficiency of ciliary cholesterol in hereditary Zellweger syndrome. *EMBO J.* **39**, e103499 (2020).
10. Poirier, Y., Antonenkov, V. D., Glumoff, T. & Hiltunen, J. K. Peroxisomal beta-oxidation-a metabolic pathway with multiple functions. *Biochim. Biophys. Acta* **1763**, 1413–1426 (2006).
11. Wanders, R. J. Metabolic functions of peroxisomes in health and disease. *Biochimie* **98**, 36–44 (2014).
12. Ferdinandusse, S., Denis, S., Van Roermund, C. W., Wanders, R. J. & Dacremont, G. Identification of the peroxisomal beta-oxidation enzymes involved in the degradation of long-chain dicarboxylic acids. *J. Lipid Res.* **45**, 1104–1111 (2004).
13. Pietrocola, F., Galluzzi, L., Bravo-San Pedro, J. M., Madeo, F. & Kroemer, G. Acetyl coenzyme A: a central metabolite and second messenger. *Cell Metab.* **21**, 805–821 (2015).
14. Ferdinandusse, S. et al. Clinical and biochemical spectrum of D-bifunctional protein deficiency. *Ann. Neurol.* **59**, 92–104 (2006).
15. van Grunsven, E. G. et al. Peroxisomal bifunctional protein deficiency revisited: resolution of its true enzymatic and molecular basis. *Am. J. Hum. Genet.* **64**, 99–107 (1999).
16. van Grunsven, E. G., Mooijer, P. A., Aubourg, P. & Wanders, R. J. Enoyl-CoA hydratase deficiency: identification of a new type of D-bifunctional protein deficiency. *Hum. Mol. Genet.* **8**, 1509–1516 (1999).
17. Nascimento, J. et al. D-bifunctional protein deficiency: a cause of neonatal onset seizures and hypotonia. *Pediatr. Neurol.* **52**, 539–543 (2015).
18. Bae, E. Y. et al. First case of peroxisomal D-bifunctional protein deficiency with novel HSD17B4 mutations and progressive neuropathy in Korea. *J. Korean Med. Sci.* **35**, e357 (2020).
19. Werner, K. M. et al. D-bifunctional protein deficiency caused by splicing variants in a neonate with severe peroxisomal dysfunction and persistent hypoglycemia. *Am. J. Med. Genet. A* **188**, 357–363 (2022).
20. Huyghe, S., Mannaerts, G. P., Baes, M. & Van Veldhoven, P. P. Peroxisomal multifunctional protein-2: the enzyme, the patients and the knockout mouse model. *Biochim. Biophys. Acta* **1761**, 973–994 (2006).
21. Verheijden, S., Beckers, L., De Munter, S., Van Veldhoven, P. P. & Baes, M. Central nervous system pathology in MFP2 deficiency: insights from general and conditional knockout mouse models. *Biochimie* **98**, 119–126 (2014).
22. De Munter, S. et al. Early-onset Purkinje cell dysfunction underlies cerebellar ataxia in peroxisomal multifunctional protein-2 deficiency. *Neurobiol. Dis.* **94**, 157–168 (2016).
23. Das, Y. et al. Peroxisomal multifunctional protein 2 deficiency perturbs lipid homeostasis in the retina and causes visual dysfunction in mice. *Front. Cell Dev. Biol.* **9**, 632930 (2021).
24. Chen, S. et al. Two novel HSD17B4 heterozygous mutations in association with D-bifunctional protein deficiency: a case report and literature review. *Front. Pediatr.* **9**, 679597 (2021).
25. Landau, Y. E. et al. Four patients with D-bifunctional protein (DBP) deficiency: expanding the phenotypic spectrum of a highly variable disease. *Mol. Genet. Metab. Rep.* **25**, 100631 (2020).
26. Pierce, S. B. et al. Mutations in the DBP-deficiency protein HSD17B4 cause ovarian dysgenesis, hearing loss, and ataxia of Perrault Syndrome. *Am. J. Hum. Genet.* **87**, 282–288 (2010).
27. Cardenas-Rodriguez, M. & Badano, J. L. Ciliary biology: understanding the cellular and genetic basis of human ciliopathies. *Am. J. Med. Genet. C Semin. Med. Genet.* **151C**, 263–280 (2009).
28. Rao Damerla, R. et al. Role of cilia in structural birth defects: insights from ciliopathy mutant mouse models. *Birth Defects Res. C Embryo Today* **102**, 115–125 (2014).
29. Wanders, R. J., Waterham, H. R. & Ferdinandusse, S. Metabolic interplay between peroxisomes and other subcellular organelles including mitochondria and the endoplasmic reticulum. *Front. Cell Dev. Biol.* **3**, 83 (2016).
30. Martin, W. F. Older than genes: the acetyl CoA pathway and origins. *Front. Microbiol.* **11**, 817 (2020).
31. Moffett, J. R., Puthillathu, N., Vengilote, R., Jaworski, D. M. & Namboodiri, A. M. Acetate revisited: a key biomolecule at the nexus of metabolism, epigenetics and oncogenesis—Part 1: acetyl-CoA, acetogenesis and acyl-CoA short-chain synthetases. *Front. Physiol.* **11**, 580167 (2020).
32. Ku, J. T., Chen, A. Y. & Lan, E. I. Metabolic engineering design strategies for increasing acetyl-CoA flux. *Metabolites* **10**, 166 (2020).
33. Sivanand, S., Viney, I. & Wellen, K. E. Spatiotemporal control of acetyl-CoA metabolism in chromatin regulation. *Trends Biochem. Sci.* **43**, 61–74 (2018).
34. Gao, X. et al. Acetate functions as an epigenetic metabolite to promote lipid synthesis under hypoxia. *Nat. Commun.* **7**, 11960 (2016).
35. Ran, J., Yang, Y., Li, D., Liu, M. & Zhou, J. Deacetylation of α-tubulin and cortactin is required for HDAC6 to trigger ciliary disassembly. *Sci. Rep.* **5**, 12917 (2015).
36. Manto, M. U. & Jissendi, P. Cerebellum: links between development, developmental disorders and motor learning. *Front. Neuroanat.* **6**, 1 (2012).
37. Prati, J. M., Guilherme, E. M., de Russo, T. L. & Gianlorenco, A. C. L. Neuronal activation of cerebellum functional circuits in motor and non-motor functions in mice. *Neurosci. Lett.* **765**, 136271 (2021).
38. De Duve, C. & Baudhuin, P. Peroxisomes (microbodies and related particles). *Physiol. Rev.* **46**, 323–357 (1966).
39. Lazarow, P. B. The role of peroxisomes in mammalian cellular metabolism. *J. Inherit. Metab. Dis.* **10**, 11–22 (1987).
40. Weller, S., Gould, S. J. & Valle, D. Peroxisome biogenesis disorders. *Annu. Rev. Genom. Hum. Genet.* **4**, 165–211 (2003).
41. Waterham, H. R., Ferdinandusse, S. & Wanders, R. J. Human disorders of peroxisome metabolism and biogenesis. *Biochim. Biophys. Acta* **1863**, 922–933 (2016).

42. De Munter, S., Verheijden, S., Régal, L. & Baes, M. Peroxisomal disorders: a review on cerebellar pathologies. *Brain Pathol.* **25**, 663–678 (2015).
43. De Munter, S. & Baes, M. Developmental and Degenerative cerebellar pathologies in peroxisomal β-oxidation deficiency. *Adv. Exp. Med. Biol.* **1299**, 105–115 (2020).
44. Galdieri, L. & Vancura, A. Acetyl-CoA carboxylase regulates global histone acetylation. *J. Biol. Chem.* **287**, 23865–23876 (2012).
45. Seto, E. & Yoshida, M. Erasers of histone acetylation: the histone deacetylase enzymes. *Cold Spring Harb. Perspect. Biol.* **6**, a018713 (2014).
46. Gradilone, S. A. et al. HDAC6 inhibition restores ciliary expression and decreases tumor growth. *Cancer Res.* **73**, 2259–2270 (2013).
47. Wallace, V. A. Purkinje-cell-derived Sonic hedgehog regulates granule neuron precursor cell proliferation in the developing mouse cerebellum. *Curr. Biol.* **9**, 445–448 (1999).
48. Spassky, N. et al. Primary cilia are required for cerebellar development and Shh-dependent expansion of progenitor pool. *Dev. Biol.* **317**, 246–259 (2008).
49. Tripathi, P. et al. Palmitoylation of acetylated tubulin and association with ceramide-rich platforms is critical for ciliogenesis. *J Lipid Res.* **62**, 100021 (2021).
50. Willemarck, N. et al. Aberrant activation of fatty acid synthesis suppresses primary cilium formation and distorts tissue development. *Cancer Res.* **70**, 9453–9462 (2010).

Acknowledgements

We thank Dr. Joon Kim (KAIST, South Korea) and Dr. Joo-Yong Lee (GRAST, South Korea) for providing RPE and *HDAC6* WT, KO MEFs, respectively. Also, we thank INFRAFRONTIER/EMMA (www.infrafrontier.eu, PMID: 25414328), and CCP-IMG (Prague, Czech Republic) for distributing the mouse line (EM: 12344). This research was supported by the Basic Science Research Program through the National Research Foundation of Korea (NRF) funded by the Ministry of Education [RS-2024-00463344]. This research was supported by the NRF of Korea, funded by the Ministry of Science & ICT [RS-2024-00338475], and by the Korea Institute for Advancement of Technology funded by the Ministry of Trade, Industry and Energy [P0025489]. This research was supported by the G-LAMP Program of the NRF grant funded by the Ministry of Education [RS-2023-00301914]. This research was also supported by the ORGASIS Corporation.

Author contributions

J.-E.B., S.J., J.B.K., H.H., D.S.J., and N.Y.P. performed the experiments, data analysis, and interpretation. H.-S.L., Z.Y.R., and D.-H.C. participated in its design and coordination. M.-S.K., H.-Y.R., H.-S.L., D.-H.C., D.-S.L., M.B., and P.K. supported research funding. J.-E.B., S.J., and D.-H.C. wrote the paper. All authors read and approved the final manuscript.

Competing interests

The authors declare no competing interests.

Additional information

Supplementary information The online version contains supplementary material available at https://doi.org/10.1038/s41467-025-57793-8.

Correspondence and requests for materials should be addressed to Zae Young Ryoo or Dong-Hyung Cho.

Peer review information *Nature Communications* thanks the anonymous reviewer(s) for their contribution to the peer review of this work. A peer review file is available.